Case Studies in Construction Materials 20 (2024) e03281

Contents lists available at ScienceDirect

Case Studies in Construction Materials

journal homepage: www.elsevier.com/locate/cscm

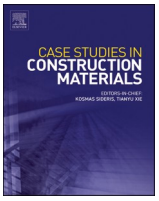

# Investigation on axial compression performance of self-compacting fly ash concrete filled square steel tube column: Tests and numerical simulation

Cun Hui *, Yangguang Wang, Zeya Ma, Shijie Lei, Ran Hai *

*School of Architecture and Civil Engineering, Zhongyuan University of Technology, Zhengzhou 450007, China*

ARTICLE INFO

*Keywords:*
Self-compacting concrete
Axial compression
Structural measures
Failure mode
Finite element analysis

ABSTRACT

Self-compacting concrete has the advantages of high fluidity, high uniform density, and low porosity. To promote the engineering application of self-compacting concrete, this article studies the axial compression test of ten square steel tube self-compacting concrete columns. The effects of design parameters such as different grades of concrete strength and internal structures of circular steel tubes, square steel tubes, and H-shaped steel on the mechanical properties of self-compacting fly ash concrete filled square steel tube columns are studied. The failure mode, characteristic load and characteristic displacement, ductility, and energy dissipation capacity of each specimen are analyzed. On the basis of the test, the finite element analysis model of steel tube self-compacting concrete column is established, and the test results and simulation results are compared and analyzed. The results show that: the failure mode of the square steel tube specimen is the multilayer middle and upper ring buckling failure. Internal structural measures of square steel tube and H-shaped steel can improve the bearing capacity, ductility, and energy dissipation capacity of the specimen. It is not recommended to use the specimen with an outer square and an inner circle design. The results of the finite element simulation have a high degree of matching with the test results, which intuitively reflects the changes in force of each component.

## 1. Introduction

Self-compacting concrete (SCC) refers to high-flowing concrete that flows automatically and is evenly filled in the formwork without external vibration [1–3]. Although the cost of SCC is higher than that of ordinary concrete [4], it can be used in projects with dense reinforcement and complex structure [5–7], effectively saving manpower and material resources in the vibration process [8], so it is preferred by researchers. Combining the advantages of steel tube and SCC, self-compacting concrete filled steel tube (SCCFST) columns are made without establishing the formwork and vibration, which can greatly improve construction efficiency and save cost [9]. At the same time, the concrete filled in the steel tube also improves the shortcomings of easy instability and buckling deformation when the pure steel tube is subjected to force. It can give full play to the characteristics of high compressive strength of concrete and good ductility of steel tube, so that the bearing capacity, stability, fire resistance and seismic capacity of the structure have been qualitatively improved [10,11].

* Corresponding authors.
*E-mail addresses:* hcun@zut.edu.cn (C. Hui), hairan@zut.edu.cn (R. Hai).

https://doi.org/10.1016/j.cscm.2024.e03281
Received 9 January 2024; Received in revised form 15 April 2024; Accepted 10 May 2024
Available online 14 May 2024

At present, many scholars have carried out the axial compression test of self-compacting concrete filled steel tube columns under different concrete mix ratio, concrete strength, steel tube wall thickness, length-diameter ratio [12–14] and other parameters. In recent years, in order to reflect the beauty of architecture, some scholars have explored the performance of circular, square or elliptical self-compacting concrete filled steel tube under axial and eccentric compression [15–17]. Especially, the axial compression tests on elliptical high strength steel tubes filled with self-compacting concrete of different mix proportions and behavior of square and rectangular concrete-filled steel tube (CFST) columns with horizontal reinforcing bars under eccentric compression have been deeply investigated [18,19]. With the development of the times and the progress of science and technology, the traditional concrete-filled steel tubular structure also needs to keep pace with the times and constantly innovate to adapt to the complex and changeable construction environment. The concrete filled steel tube under the complex form has higher ductility and strength performance. Although some scholars have carried out complex design of ordinary concrete-filled steel tube columns, such as outer circle and inner square, outer square and inner square, special-shaped steel tube, outer steel tube reinforcement and other forms [20–24], there are only a few studies on self-compacting concrete filled square steel tube under complex forms.

In this experiment, the type of concrete, the strength grade of concrete and the internal structural measures were taken as the main variables. The axial compression test of 10 square steel tube self-compacting concrete columns was carried out. On the basis of experimental research, ABAQUS was used to establish the numerical analysis model of steel tube fly ash self-compacting concrete columns under axial compression. The failure mode of square steel tube self-compacting concrete columns under axial compression can provide some reference for the study of axial compression performance of complex forms of steel tube concrete columns, and provide some theoretical support for related engineering applications.

## 2. Test program

### 2.1. Mix proportions and properties of concrete

The raw materials of ordinary SCC are cement, coarse aggregate, fine aggregate, water, and water reducing agent. SCFAC is made by replacing cement with fly ash in a certain proportion on the basis of ordinary SCC. The relevant performance tests are carried out. The test results are shown in Table 1. The self-compacting concrete produced meets the requirements of the specification [25]. The detailed information of each raw material is as follows: the cement used is P.O 42.5 ordinary Portland cement; the fly ash is grade II fly ash; coarse aggregate is a continuous graded gravel with a particle size of 5–20 mm; the fine aggregate is a natural river sand with a fineness modulus of 2.3 and a standard sieve; the water reducer uses high-efficiency polycarboxylate superplasticizer and the water reduction efficiency is 30 %. Water is laboratory tap water. Two kinds of SCC with different NC40 and NC60 strength were made. On this basis, two kinds of SCFAC with FA40 and FA60 strength were produced using fly ash to replace cement in a fixed proportion. The cooperation of each group is shown in Table 2.

### 2.2. Specimen design

In this experiment, the concrete strength grade and internal structural measures are taken as the main variables to compare the axial compression performance of the SCFACFST columns and the ordinary SCCFST columns. A total of 10 square SCCFST columns with a height of 700 mm were designed, of which 2 were ordinary SCCFST columns and the remaining 8 were SCFACFST columns. The side length of the outer square steel tube is 200 mm × 200 mm. The internal structure adopts a circular steel tube with a diameter of 90 mm, a square steel tube with a side length of 80 mm × 80 mm, and an H-shaped steel with a side length of 90 mm × 90 mm × 4 mm × 4 mm. The steel tubes are all ordinary Q235B steel pipes produced in the same batch. The nominal wall thickness t of the steel tube is 4 mm, the yield strength is 279 MPa, the ultimate strength is 394 MPa, the elongation is 30.6 %, and the yield ratio is 0.7. The internal structure is shown in Fig. 1, and the detailed design parameters are shown in Table 3.

### 2.3. Loading scheme

The test is completed on a 5000 kN electro-hydraulic servo universal testing machine, and the loading device is shown in Fig. 2. The test loading is divided into two stages: preloading and formal loading. First, preloading is performed, and 10 % of the estimated ultimate load is applied and maintained for 1 minute. During this period, data acquisition is verified to confirm that the equipment is fully unloaded after normal operation and enters the formal loading stage. Formal loading is displacement-controlled loading. The continuous loading method is adopted. The loading rate is set at 0.4 mm/ min. When the longitudinal displacement reaches 50 mm, the steel pipe weld cracks and the bearing capacity decreases significantly, the loading is stopped and the test ends.

**Table 1**
Test results of workability and mechanical properties of self-compacting concrete.

| Types of concrete | Slump flow/mm | J-ring flow/mm | $T_{500}$/s | Gap passability/mm | $f_{cu}$/MPa |
|---|---|---|---|---|---|
| NC40 | 650 | 635 | 4.6 | 15 | 49.7 |
| NC60 | 640 | 625 | 4.9 | 15 | 69.8 |
| FA40 | 690 | 670 | 3.2 | 20 | 48.5 |
| FA60 | 685 | 660 | 2.9 | 25 | 67.1 |

**Table 2**
Mix proportion of SCC (Unit: kg/m$^3$).

| Specimen | Water cement ratio | Cement | Fly ash | Coarse aggregate | Fine aggregate | Water | Water reducer |
|---|---|---|---|---|---|---|---|
| NC40 | 0.37 | 486.5 | 0 | 950 | 809.6 | 180 | 4.87 |
| NC60 | 0.31 | 516 | 0 | 909 | 774 | 160 | 7.74 |
| FA40 | 0.37 | 291.9 | 194.6 | 950 | 809.6 | 180 | 4.87 |
| FA60 | 0.31 | 309.6 | 206.4 | 909 | 774 | 160 | 7.74 |

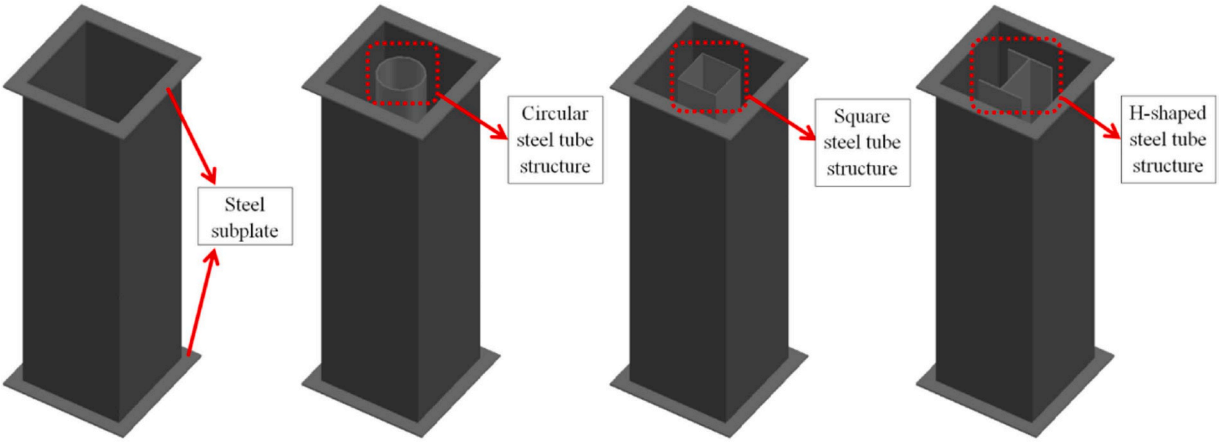


**Fig. 1.** Internal structure of specimen.

**Table 3**
Design parameters for each specimen.

| Specimen | Sectional dimension/mm | Strength grade of concrete | Internal structure form | Cross sectional area/mm$^2$ | Steel area/mm$^2$ | Steel ratio |
|---|---|---|---|---|---|---|
| NC40-S | 200 × 200 | NC40 | — | 40,000 | 3136 | 7.8 % |
| NC60-S | 200 × 200 | NC60 | — | 40,000 | 3136 | 7.8 % |
| FA40-S | 200 × 200 | FA40 | — | 40,000 | 3136 | 7.8 % |
| FA40-S-C | 200 × 200 | FA40 | Circular steel tube | 40,000 | 4216 | 10.5 % |
| FA40-S-H | 200 × 200 | FA40 | H-shaped steel | 40,000 | 4216 | 10.5 % |
| FA40-S-S | 200 × 200 | FA40 | Square steel tube | 40,000 | 4352 | 10.9 % |
| FA60-S | 200 × 200 | FA60 | — | 40,000 | 3136 | 7.8 % |
| FA60-S-C | 200 × 200 | FA60 | Circular steel tube | 40,000 | 4216 | 10.5 % |
| FA60-S-H | 200 × 200 | FA60 | H-shaped steel | 40,000 | 4216 | 10.5 % |
| FA60-S-S | 200 × 200 | FA60 | Square steel tube | 40,000 | 4352 | 10.9 % |

## 3. Test results and analysis

### 3.1. Test phenomena

The failure mode of each sample is shown in Fig. 3.
It can be seen from Fig. 3:

(1) The failure mode of all square SCCFST column specimens is a typical multilayer ring buckling failure, and the failure position is concentrated in the middle and upper part of the specimen. The concrete manifestation is that the multilayer continuous ring buckling appears in the middle and upper part of the square steel tube, and the first layer ring buckling first appears closer to the top of the specimen. The internal structural measures and the type and strength of concrete do not have a significant effect on the deformation and failure state of the square SCCFST column specimens.
(2) SCCFST column specimens from all parties show multi-layer ring buckling failure. In the initial loading stage, the specimen is in the elastic stage under load, and the appearance does not show obvious changes. According to the load-specimen curves shown in Fig. 4(a), the load in the elastic stage increases linearly. At about 80 % of the peak load, the specimen intermittently appears with the sound of concrete fragmentation. The peak load of each SCCFST column specimen generally appears in the vertical displacement range of 7–10 mm, and slight deformation occurs on some surfaces. After that, with increasing vertical displacement, the specimen deformation intensified and the buckling deformation visible to the naked eye appeared successively on each side, gradually converged into a continuous ring buckling and continuously made the buckling full. At this time,

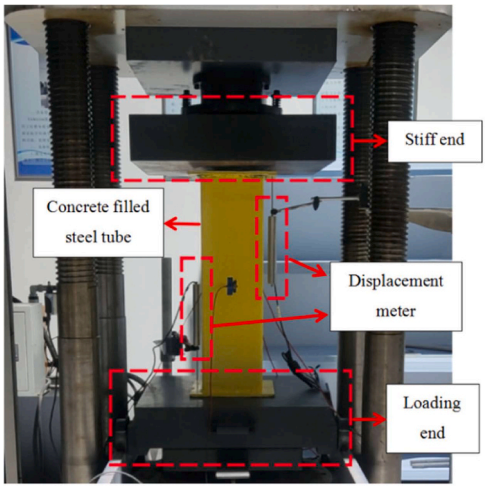


**Fig. 2.** Loading device.

the bearing capacity had gradually decreased. Generally, the annular buckling of the second layer appears slowly after 25 mm. Similarly to the first layer, it first appears on some surfaces and continues to expand and converge until the buckling positions of each side are connected to each other. At this time, the bearing capacity of each specimen has basically stabilized. With increasing vertical displacement, the surface deformation of the specimen increases and the bearing capacity may rebound slightly, but it has little effect on the test results.

(3) During the test, the specimen was continuously observed and the hollowing state of the specimen was judged by the knocking method. The adhesion between the square steel tube and the SCC is relatively poor, and it is easy to appear that the phenomenon of hollowing is occurring. This is because the square steel tube is easy to cause the large area peeling of the steel tube and the SCFAC when the bulging deformation occurs. With the continuous action of the load, the hollowing phenomenon will soon end. The SCFAC is crushed and reorganized, which can effectively fill the gap between the steel tube and the concrete, and make the steel tube and the SCFAC closely combined.

### *3.2. Load-displacement curve*

The load-displacement curve of the specimen is shown in Fig. 4. In the figure, *F* represents the load on the specimen, the direction is vertical and upward, and the compression is positive; *U* represents the vertical displacement of the specimen, which is positive upward.

It can be seen from Fig. 4 that:

(1) The load-displacement curves of each specimen are similar. Before reaching the peak load, the load and displacement are basically linear, and the yield stage is not obvious enough. After reaching peak load, each SCFACFST column specimen begins to decline to varying degrees. After falling to a certain load, due to the buckling of the specimen, the stress area increases and the load increases slightly. However, in general, it does not have a significant effect on the bearing performance of the specimen and the deformation of the specimen at this stage is too obvious and is no longer suitable for continuous bearing. The load-displacement curves of the specimens FA40-S-C and FA60-S-C are obviously different from those of other specimens. The load growth rate of specimen FA40-S-C slows down when the displacement is about 5 mm, then increases rapidly to a stable state again until 7.5 mm, and then basically remains at a stable stage. The bearing capacity of the specimen FA60-S-C decreases slightly and remains at a high level after reaching the peak load, and with the increase in the deformation of the specimen, the bearing capacity increases slightly beyond the peak load, but the displacement has reached 40 mm, the deformation of the sample is significant, and there is no practical reference value.

(2) The use of square steel tubes and H-shaped steel in the internal structure can significantly improve the bearing capacity of the specimen. Different internal structural measures have a great influence on the bearing capacity of the specimens. The specimens with internal structural measures of square steel tube and H-shaped steel have better bearing capacity than those with internal structural measures of circular steel tube. Taking the C60 strength specimen as an example, the peak load of the specimens with internal structural measures of square steel tube, H-shaped steel tube and circular steel tube is increased by 9.3 %, 7.4 % and-9.2 % respectively compared with the specimens without internal structural measures. The selection of the internal structure should be determined according to the actual situation. But the structural measures of adding the inner circular steel tube to the outer square steel tube are not suitable for the actual project and should be avoided.

(3) Taking concrete type as a variable, the strength of SCFAC specimens FA40 with 28d strength grade reaching the C40 standard is greater than that of ordinary SCC specimens NC40 at long age. Fly ash with an appropriate replacement rate has a positive effect on improving the strength of self-compacting concrete, and this phenomenon is more significant under the constraint of steel

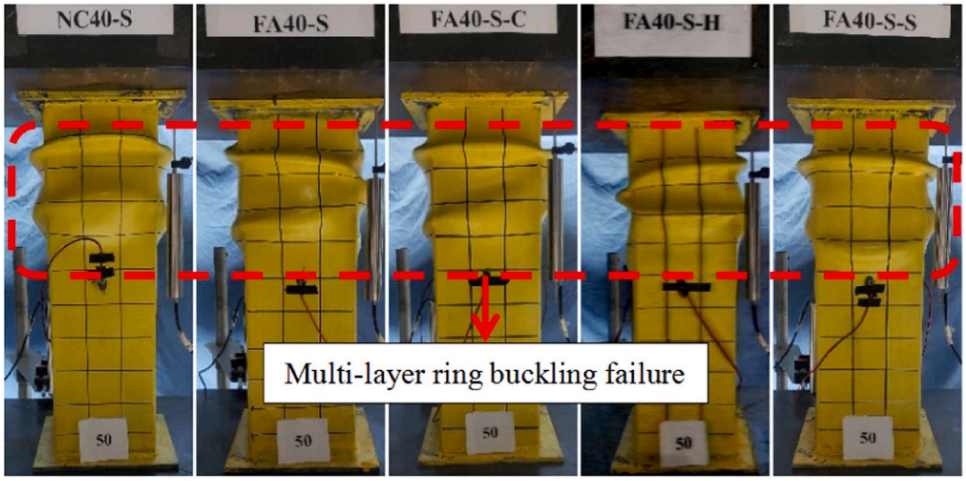


(a) C40 specimens

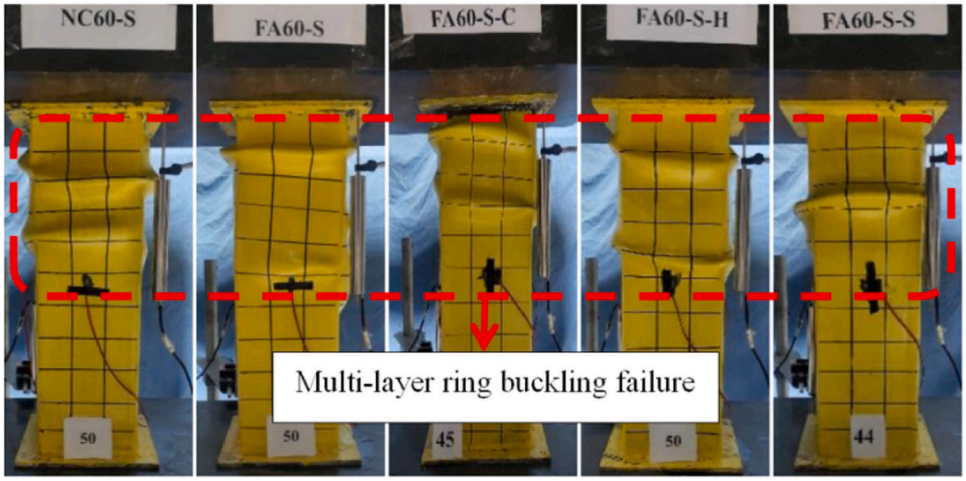


(b) C60specimens

**Fig. 3.** Failure modes of square steel tubes.

tube. SCFAC specimens FA60 whose 28 d strength grade reaches the C60 standard has little difference with the strength growth of ordinary SCC specimens NC60 at long age. This is due to the small water-cement ratio of C60 SCC and the large amount of cement. Fly ash cannot completely replace cement to produce strength. The large replacement rate of fly ash will lead to weakening of the long-term performance of the SCC. Combined with the results of this experiment, it is suggested that the replacement rate of fly ash in high-strength concrete should not be higher than 40 %.

### *3.3. Characteristic load and characteristic displacement*

To study the deformation and failure mechanism of SCFACFST columns under axial load, the yield load, peak load, ultimate load and corresponding displacement of each specimen are taken as characteristic parameters for analysis. The influence of concrete strength grade, outer steel tube type, and internal structure form is discussed. The summary of each characteristic parameter is shown in Table 4.

Combined with the load-displacement curves of each specimen and Table 4, the following conclusions can be obtained:

(1) The bearing capacity of each specimen is maintained at a high level due to the addition of concrete. When subjected to external loads, due to the restraint of the steel tube, the concrete is in a three-dimensional stress state in the steel tube, and its high compressive strength is fully utilized. At the same time, the concrete filled in the steel tube can effectively avoid the buckling failure of the steel tube. The steel tube and the fly ash self-compacting concrete bear the load together, giving full play to the respective advantages of the two materials.

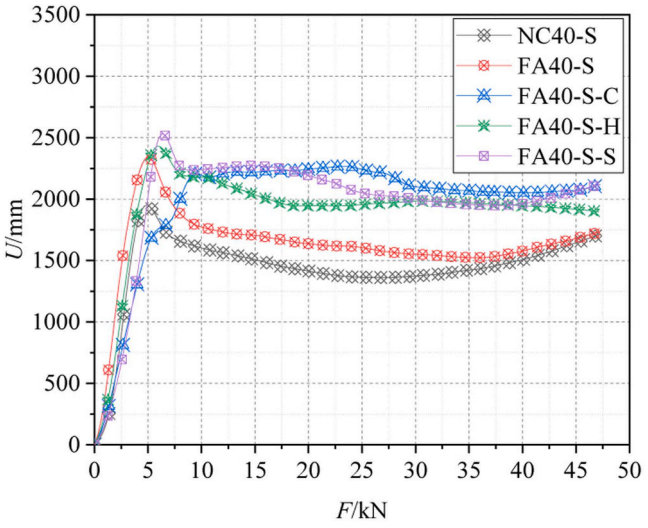


(a) C40 specimens

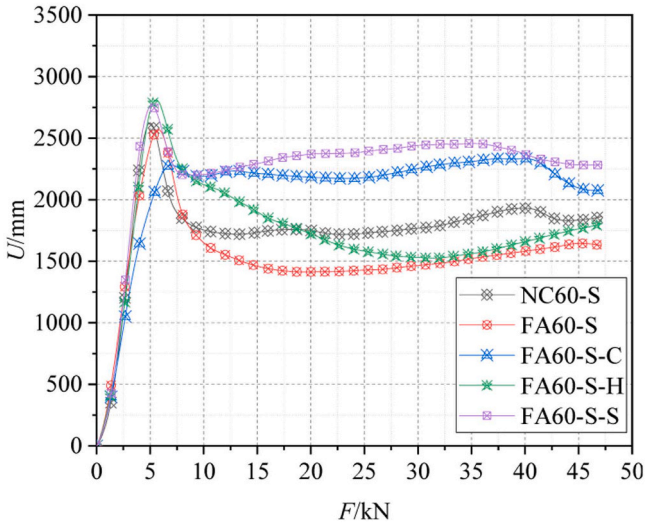


(b) C60 specimens

**Fig. 4.** Load-displacement curves of each specimen.

**Table 4**
Characteristic load and characteristic displacement.

| Specimen | Yield load/ kN | Yield displacement/ mm | Peak load/ kN | Peak displacement/ mm | Ultimate load/ kN | Ultimate displacement/ mm | Ductility factor |
|---|---|---|---|---|---|---|---|
| NC40-S | 1595.39 | 6.14 | 1950.18 | 5.60 | 1696.88 | 10.88 | 1.77 |
| NC60-S | 2170.08 | 6.47 | 2623.04 | 5.71 | 2302.63 | 9.02 | 1.39 |
| FA40-S | 1932.81 | 5.70 | 2338.59 | 5.55 | 2056.79 | 9.61 | 1.69 |
| FA40-S-C | 1819.69 | 8.23 | 2266.21 | 9.92 | 2245.73 | 13.16 | 1.60 |
| FA40-S-H | 2028.26 | 6.48 | 2430.33 | 6.40 | 2151.32 | 16.93 | 2.61 |
| FA40-S-S | 2081.46 | 7.75 | 2530.76 | 7.13 | 2214.40 | 24.88 | 3.21 |
| FA60-S | 2141.34 | 6.70 | 2570.68 | 6.52 | 2276.58 | 9.89 | 1.48 |
| FA60-S-C | 1901.11 | 7.14 | 2333.52 | 7.65 | 2269.85 | 25.01 | 3.50 |
| FA60-S-H | 2330.28 | 6.72 | 2810.81 | 6.19 | 2474.95 | 9.91 | 1.47 |
| FA60-S-S | 2280.10 | 6.46 | 2761.91 | 5.91 | 2427.18 | 9.69 | 1.50 |

(2) Construction measures also have a certain influence on the bearing capacity of each specimen, but they play no decisive role. The internal structure of the specimen FA40-S-C and the specimen FA60-S-C is unfavorable to the bearing capacity of the specimen. Compared to the bearing capacity of the specimen FA40-S and FA60-S without structural measures, the bearing capacity of the specimen FA40-S-C and FA60-S-C is worse. Combined with the actual peak load of the specimen, the peak load of FA40-S-C and FA60-S-C is 2266.21 kN and 2333.52 kN, respectively, while the peak load of FA40-S and FA60-S is 2338.59 kN and 2570.68 kN, respectively. The weakening amplitude of the peak load is 3.1 % and 9.2 %, respectively. This is because when the square SCCFST column is added to the circular steel tube structure, the thickness of the sandwich concrete is not uniform, and the bearing performance of the square SCCFST column is worse than that of the circular steel tube specimen, and the constraint effect is relatively low, resulting in the concrete being more likely to appear. The weak position of the force accelerates the damage, and deterioration of bearing performance occurs, which not only causes waste of steel, but also reduces the safety of the stressed structure. In practical engineering, this kind of situation should be avoided as much as possible.

(3) The type and strength grade of concrete have a certain influence on the bearing capacity of the specimen. In this experiment, two ordinary SCCFST columns, NC40-S and NC60-S, were made and compared with the specimens FA40-S and FA60-S. It can be seen from Table 3 that the ultimate load of NC40-S and FA40-S specimens with different concrete types increased by 21.2 %, but the peak load of NC60-S specimens increased by 1.1 % compared to FA60-S specimens, indicating that the bearing capacity of SCFACFST columns was better than that of ordinary SCCFST columns under low strength. The improvement of the grade of the concrete strength can significantly improve the bearing capacity of the specimen. Taking the specimens NC40-S, NC60-S and FA60-S-H, FA60-S-H as an example, the ultimate load is increased by 35.7 % and 35.1 %, respectively.

### 3.4. Ductility analysis

Ductility is an important index to reflect the deformation capacity of members. The displacement ductility coefficient is positively correlated with the deformation capacity. The larger the value, the better the deformation performance. Considering the safety of the structure, the CFST column should have sufficient deformation capacity and have obvious deformation before the failure of the specimen, so as to avoid brittle failure. The ratio of ultimate displacement to yield displacement μ represents the coefficient of ductility and is used to define the ductility of the component, as shown in Eq. (1). When the bearing capacity of the specimen reaches 80 % of the peak load in the rising stage, the corresponding load is defined as the yield load, and the corresponding displacement is the yield displacement. Due to the special trend of the load-displacement curve of some specimens, the load has been maintained at a high level. When one of the conditions disappears, it is used as the ultimate load: 1) The bearing capacity of the specimen is reduced to 85 % of the peak load. 2) After reaching the peak load, the bearing capacity of the specimen is maintained at a certain level or slightly increased after decreasing, such as FA40-S-C and FA60-S-C. According to the strength retention phenomenon, the minimum load at this stage is selected as the ultimate load. 3) The surface deformation of the specimen is obvious, and it is not suitable to continue to bear the load. The ultimate displacement is the displacement corresponding to the ultimate load obtained according to the above conditions.

$$\mu = \Delta_u / \Delta_y \tag{1}$$

In the formula, $\Delta_u$ represents the ultimate displacement and $\Delta_y$ represents the yield displacement.
The results of the calculation of the ductility coefficient of each specimen are summarized in Table 4. It can be seen in Table 4:

(1) The ductility coefficient of each specimen is concentrated between 1.39 and 3.50, with an average of 2.02. The specimen has sufficient deformation development from yield to failure, and the failure mode is not sudden brittle failure, showing good deformation ability.

(2) Selecting the appropriate internal structure will improve the ductility of the CFST columns, and the degree of ductility improvement caused by different structural measures is slightly different. Taking FA40-S, FA40-S-C, FA40-S-H and FA40-S-S as examples, after adding structural measures, the ductility of CFST columns is increased by-9 %, 24.3 % and 90 %, respectively. Appropriate addition of structural measures can effectively improve the ductility of CFST column specimens.

(3) The type and strength of the SCC have little effect on the ductility of the structure. The ductility coefficient of SCCFST columns with different grades of concrete strength is not much different. It should be noted that the specimen FA40-S-C and FA60-S-C show very different ductility changes. This is because the two have maintained a high level of load bearing capacity. The ultimate load and the ultimate displacement are based on empirical values, so they show different changes. The ductility change of the specimen is only for reference and needs further study.

### 3.5. Analysis of energy consumption

Total energy absorption $E$, average compression force $F_m$ and compression force efficiency $\eta$ are commonly used evaluation indexes for structural energy dissipation capacity. Under the action of external load, the CFST column will produce a continuous cumulative deformation. At this stage, the total energy absorbed by the specimen to produce deformation of buckling and concrete crushing and reorganization is defined as the total energy absorption $E$, the unit is J; the ratio of the total energy absorption $E$ to the vertical displacement generated by the specimen is called the average compression force $F_m$, which reflects the applied load required for the unit displacement of the specimen. The ratio of the average compression force $F_m$ to the peak load is called the compression force efficiency $\eta$. The closer the compression force efficiency is to 1, the closer the average compression force is to the peak load, and the

higher the utilization efficiency of the material. The total energy absorption $E$, the average compression force $F_m$ and the compression force efficiency $\eta$ are calculated as follows:

$$E = \int_0^U F d\delta \tag{2}$$

$$F_m = E/U \tag{3}$$

$$\eta = F_m/F_p \tag{4}$$

In the formula, $U$ is the vertical displacement of the specimen, the unit is mm, $F$ is the load borne by the specimen, $F_p$ is the peak load borne by the specimen, and the unit is kN.

From Table 5 we can see that:

(1) The internal structure has an obvious effect on the energy dissipation capacity of the specimen, and the effect of different structural measures is different. From the test results of each group, the energy dissipation capacity of embedded H-shaped steel, circular steel tube and square steel tube increases in turn. Taking FA60-S-H, FA60-S-C and FA60-S-S as examples, it can be seen that the total energy absorption of FA60-S-H is 11.1 %, 32.8 % and 42.2 % higher than that of FA60-S, but the compression force efficiency of FA60-S-H is obviously abnormal from that of other groups. This is because the deformation of this specimen intensifies at the later stage of loading, and the bearing capacity obviously decreases, resulting in a significant decrease in the efficiency of total energy absorption and compression force compared to other groups.

(2) The influence of concrete type and strength. When the concrete strength is C40, the total energy absorption of the specimen is improved, but the compression force efficiency is decreased, indicating that the strength of the SCFAC in the strength grade is higher and the unit displacement needs to absorb more energy; when the concrete strength is C60, the total energy absorption and compressive force efficiency of the two groups of specimens decrease. Compared to NC60-S, the total energy absorption of FA60-S decreases by 10.7 %, and the compressive force efficiency decreases by 9.7 %. SCFAC and ordinary SCC under different strength show different energy dissipation capacities. This is due to the increase of the concrete strength grade; the strength provided by fly ash is not enough to make up for the strength provided by cement hydration. In high-strength concrete, the replacement rate of fly ash should be appropriately reduced to ensure the safety of the structure in long-term use. When the concrete strength grade is only used as a variable, the higher the SCFAC strength, SCFAC the greater the total energy absorption of the specimen and there is no significant difference in the compression force efficiency. In practical application, the appropriate concrete strength should be selected according to the use situation.

## 4. Numerical analysis

### 4.1. Model establishment

In the actual test process, the stress and deformation of the internal components can't be observed intuitively. There are some limitations for observing the structural behavior of sandwich concrete, internal steel pipe or steel, and core concrete. Therefore, ABAQUS software is used to establish a finite element model and analyze the mechanism. The thin-walled steel tube adopts the four-node S4R shell element and the concrete adopts the eight-node linear hexahedral element C3D8R solid element. When considering the interaction between the components, the binding constraints are used between the steel tube and the cover plate and between the concrete and the cover plate. The surface of the cover plate is coupled to the reference point in the center of the cover plate to facilitate load application. The upper end of the CFST column is applied with fixed constraints, and the vertical displacement of the $Z$ axis is applied at the lower end.

For the specimens filled steel tubes, the models of sandwich concrete and core concrete need to be established, respectively. The ends of each component are bound to the upper and lower cover plates, respectively, and the contact definition is used between the

**Table 5**
Evaluation index of energy dissipation capacity of specimens.

| Specimen | Total energy absorption $E$/J | mean crush load $F_m$/kN | Peak load $F_p$/kN | Crash load efficiency $\eta$ |
|---|---|---|---|---|
| NC40-S | 70,427.34 | 1408.55 | 1950.18 | 0.71 |
| NC60-S | 87,227.91 | 1744.56 | 2623.04 | 0.64 |
| FA40-S | 80,874.17 | 1617.48 | 2338.59 | 0.67 |
| FA40-S-C | 97,503.14 | 1950.06 | 2266.21 | 0.86 |
| FA40-S-H | 96,044.18 | 1920.88 | 2430.33 | 0.76 |
| FA40-S-S | 96,481.98 | 1929.64 | 2530.76 | 0.74 |
| FA60-S | 77,880.11 | 1557.60 | 2570.68 | 0.58 |
| FA60-S-C | 103,449.34 | 2068.99 | 2333.52 | 0.87 |
| FA60-S-H | 86,495.92 | 1729.92 | 2810.81 | 0.59 |
| FA60-S-S | 110,760.38 | 2215.21 | 2761.91 | 0.78 |

components. Due to the small wall thickness of the steel tube, concrete is used as the main surface. Steel-filled specimens are simulated by the 'built-in area '.

In this simulation, concrete is the main surface, and the surface-surface contact interaction is adopted between the steel tube and the concrete. The contact tolerance is set to 0.1; the normal behavior adopts hard contact, allowing separation after contact; the tangential behavior is based on the Coulomb friction model, the penalty function is introduced, and the friction coefficient is 0.6. The cover plate obeys the linear elastic model, the elastic modulus is $1.0 \times 10^9$ GPa, the Poisson ratio is $1.0 \times 10^{-5}$. The steel adopts the five-stage constitutive model, the schematic diagram is shown in Fig. 5, and the expression is shown in formula (5).

$$\sigma_s = \begin{cases} E_s\varepsilon_s & \varepsilon_s \le \varepsilon_e \\ -A\varepsilon_s^2 + B\varepsilon_s + C & \varepsilon_e < \varepsilon_s \le \varepsilon_{e1} \\ f_y & \varepsilon_{e1} < \varepsilon_s \le \varepsilon_{e2} \\ f_y[1 + 0.6(\varepsilon_s - \varepsilon_{e2})/(\varepsilon_{e3} - \varepsilon_{e2})] & \varepsilon_{e2} < \varepsilon_s \le \varepsilon_{e3} \\ 1.6f_y & \varepsilon_s > \varepsilon_{e3} \end{cases} \tag{5}$$

Where $\sigma_s$ and $\varepsilon_s$ represent the stress and strain of steel respectively, $f_y$ and $E_s$ represent the yield strength and elastic modulus of steel respectively, $\varepsilon_e$ is the strain corresponding to the proportional limit, and its expression is: $\varepsilon_e = 0.8f_y/E_s$, $\varepsilon_{e1} = 1.5\varepsilon_e$, $\varepsilon_{e2} = 10\varepsilon_e$, $\varepsilon_{e3} = 100\varepsilon_e$; $A = 0.2f_y/(\varepsilon_{e1} - \varepsilon_e)^2$, $B = 2A\varepsilon_{e1}$, $C = 0.8f_y + A\varepsilon_e^2 - B\varepsilon_e$

The damage plasticity model was used to simulate the SCFAC. Combined with the concrete constitutive relationship proposed in the references [26–28], the constitutive relationship of SCFAC in this article is as follows:

$$y = \begin{cases} 2x - x^2 & (x \le 1) \\ x/[\beta_0(x-1)^\eta + x] & (x > 1) \end{cases} \tag{6}$$

Where $x = \frac{\varepsilon}{\varepsilon_0}$, $y = \frac{\sigma}{\sigma_0}$, $\xi = \frac{A_s f_y}{A_c f_c}$, $\sigma_0 = f_c$, $f_c$ is the compressive strength of the SCFAC cylinder, the unit is N/mm$^2$, $\varepsilon_0 = \varepsilon_c + 800 \cdot \xi^{0.2} \cdot 10^{-6}$, $\varepsilon_c = (1300 + 12.5 \cdot f_c) \cdot 10^{-6}$; $\eta = 1.6 + 1.5/x$; $\beta_0 = \frac{f_c^{0.1}}{1.2\sqrt{1+\xi}}$。

### 4.2. Analysis of results

The numerical analysis model of each specimen is established respectively. The calculated stress cloud diagram of each component of the steel tube fly ash self-compacting concrete column, the comparison diagram of the load-displacement curve obtained by numerical simulation and experimental test are shown in Fig. 6, where Test represents the test curve and FEM represents the simulated curve.

From Fig. 6, it can be seen that:

(1) In general, the simulation results for finite elements agree well with the experimental phenomena. There are some differences between the failure modes of some specimens in the test and the simulation results, which are manifested mainly in the bulging position and the number of annular bulging layers. The actual failure mode of each specimen is mainly concentrated in the middle and upper parts of the specimen, which is manifested by the multilayer ring buckling in the middle and upper parts of the specimen. The failure position of the simulation results is concentrated in the middle of the specimen. From the middle of the specimen to the two ends of the specimen, there is a multilayer annular buckling. The internal structure has little effect on the

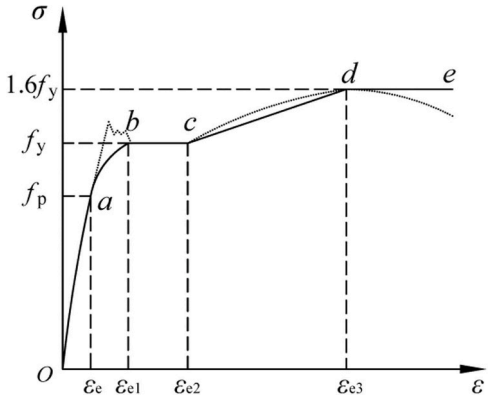


**Fig. 5.** Constitutive relationship of steel.

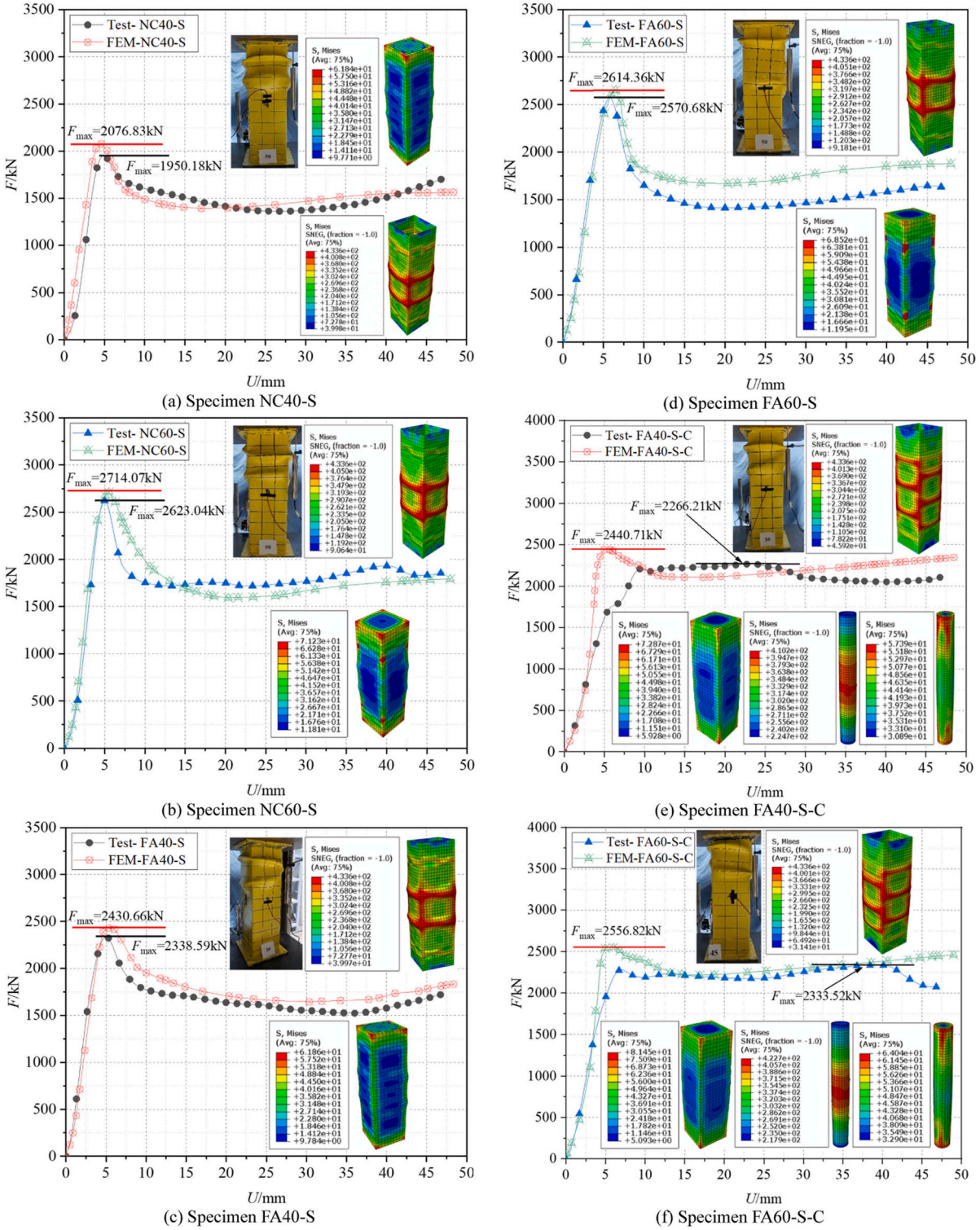


**Fig. 6.** The stress cloud diagram and test load-displacement curve of each specimen are compared with the simulation results.

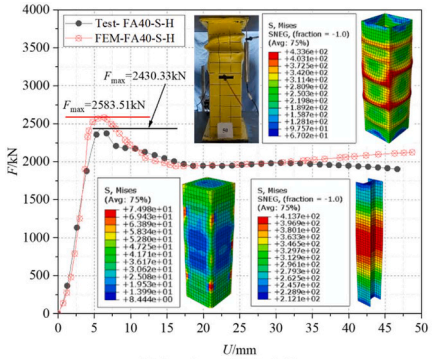


(g) Specimen FA40-S-H

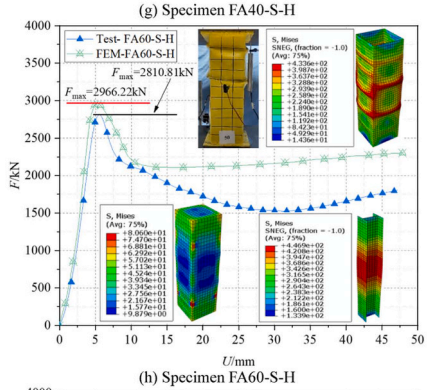


(h) Specimen FA60-S-H

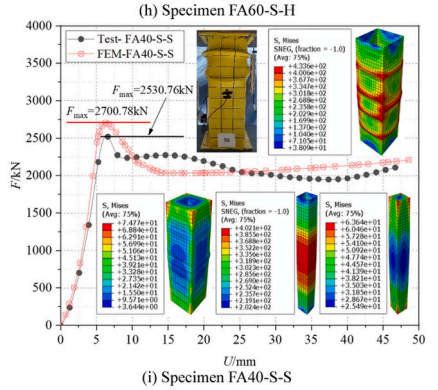


(i) Specimen FA40-S-S

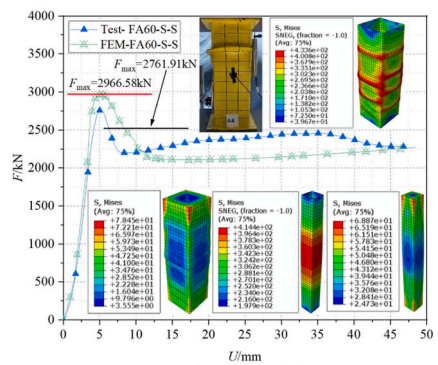


(j) Specimen FA60-S-S

**Fig. 6.** (*continued*).

failure mode of the outer square steel tube specimen. The maximum stress position of the inner filled circular steel tube, H-shaped steel tube, and square steel tube appears in the middle.

(2) The strength of concrete has no significant effect on the failure mode of SCFACFST columns. The sandwich concrete and the core concrete of each specimen have an obvious stress concentration at the upper and lower ends, and the specimen is more

significant at the corners. When observing the concrete stress cloud diagram in each specimen, it can be seen that the stress of concrete in the middle of each side of the specimen is small and the stress concentration at the corner is obvious, which is consistent with the experimental observation process.

(3) Compared to sandwich concrete, the average stress of core concrete is higher and the effect of strength improvement is better, such as specimen FA40-S-C and FA60-S-C.

### *4.3. Comparison of experimental and simulated load-displacement curves*

As can be seen from Fig. 6:

(1) Except for the specimens FA40-S-C and FA60-S-C, the load-displacement curves measured by the other specimens have the same development trend as the curves obtained by the finite element simulation, and the curve fitting degree is high. The difference between the simulated peak load and the test peak load is within 5 %. The load and displacement of each specimen increased linearly before reaching the peak load, and the growth rate slowed after the specimen was collected. However, due to continuous displacement loading, the yield stage of each specimen was not obvious. After reaching the peak load, the bearing capacity of the specimen gradually decreases, and the rate of decrease gradually decreases. When the load decreases to a certain value, there is a slight increase, which has no significant effect on the test results.

(2) The finite element simulation results are more idealized. The curves of all specimens are consistent, and there are obvious rising section, falling section and stable holding section. However, the specimens FA40-S-C and FA60-S-C are not typical due to test errors, specimen production quality, structural form and other reasons. The curves of the two specimens measured in the test are only the rising section and the stable holding section, both of which are stable after reaching the peak load and almost no downward trend, resulting in a certain difference between the simulation curve and the test curve. It should be noted that the test peak load of the specimen FA40-S-C and FA60-S-C is almost the same as the load of the smooth section of the simulated curve. In the test, the specimen fails to reach the theoretical ultimate load and directly enters the smooth holding section. Therefore, the specimen of this kind of structure still needs to further study its mechanism of action.

(3) The research in this paper is carried out under the condition that the parameters of steel pipe wall thickness and aspect ratio are unchanged, and the depth and breadth of the research content are not comprehensive enough. It is necessary to further study the eccentric compression, bending-torsion, compression-bending-shear-torsion and seismic performance of steel tube self-compacting concrete columns under more steel tube size and section type parameters. Moreover, the mechanical properties of fly ash self-compacting concrete filled steel tube columns under multi-disaster coupling need to be further studied, such as fire-impact coupling, sulfate erosion-freeze-thaw coupling and fire-earthquake coupling.

## 5. Conclusions

Ten SCCFST column specimens were designed for experimental research. The bearing capacity, ductility, and energy consumption of SCCFST under different design parameters were analyzed, and the bearing capacity of each specimen under axial load was explored. The conclusions of this paper are as follows.

(1) The failure mode of the square SCCFST column under axial compression test is multilayer ring buckling in the middle and upper part; the internal structure has a certain mitigation effect on the failure mode, while the type and strength of concrete have little effect on the failure mode.

(2) The use of square steel tubes and H-shaped steel in the internal structure of the specimen can significantly improve the bearing capacity of the specimen. The peak load of square steel tube and H-beam specimens with internal structure is 9.34 % and 7.44 % higher than that of nonstructural samples, respectively, but the structural measures with internal circular steel tube are not suitable for practical engineering. Improving the strength grade of concrete can significantly improve the bearing capacity of the specimens. Taking the specimens NC40-S, NC60-S, FA60-S-H and FA60-S-H as examples, the ultimate load is increased by 35.7 % and 35.1 %, respectively.

(3) Appropriate internal structural measures can improve the ductility and energy dissipation capacity of the specimens. The ductility coefficient of each specimen is concentrated between 1.39 and 3.50, with an average value of 2.02, showing good deformation ability. Taking FA40-S, FA40-S-C, FA40-S-H and FA40-S-S as examples, after adding structural measures, the ductility of CFST columns is increased by −9 %, 24.3 % and 90 % respectively, and the total energy absorption is increased by 32.8 %, 11.1 %, and 42.2 %. However, the type and strength of SCC have little effect on the ductility of the structure.

(4) Except for the specimen with internal structure of circular steel tube. The simulation results of finite elements have a high degree of matching with the test results. Failure modes are similar, and the stress changes of each component can be intuitively obtained. The accuracy of the numerical analysis model of the SCFACFST column and the accuracy of the finite element modeling method of complex CFST are verified. The analysis of design parameters based on this model can improve the research efficiency of this kind of CFST column, save research time and cost, and provide some technical support for experimental research and engineering application of this kind of components.

## CRediT authorship contribution statement

**Shijie Lei:** Investigation, Data curation. **Zeya Ma:** Visualization, Investigation. **Yangguang Wang:** Writing – original draft, Investigation, Conceptualization. **Cun Hui:** Writing – review & editing, Funding acquisition, Conceptualization. **Ran Hai:** Writing – review & editing.

## Declaration of Competing Interest

The authors declare that they have no known competing financial interests or personal relationships that could have appeared to influence the work reported in this paper.

## Data availability

Data will be made available on request.

## Acknowledgments

This study is funded by the National Natural Science Foundation of China (52208226).

*Conflicts of interest*

The authors declare that they have no conflicts of interest.

## References

[1] T.A. Tawfik, M. Slaný, M.T. Palou, Influence of heavyweight aggregate on the fresh, mechanical, durability, and microstructural properties of self-compacting concrete under elevated temperatures, J. Build. Eng. 80 (2023) 108104, https://doi.org/10.1016/j.jobe.2023.108104.
[2] H. Okamura, M. Ouchi, Self-compacting concrete, J. Adv. Concr. Technol. 1 (1) (2003) 5–15, https://doi.org/10.3151/jact.1.5.
[3] M.D. Rao, S. Dey, B.P. Rao, Characterization of fiber reinforced self-compacting concrete by fly ash and cement, Chem. Inorg. Mater. 1 (2023) 100010, https://doi.org/10.1016/j.cinorg.2023.100010.
[4] M. Nehdi, M. Pardhan, S. Koshowski, Durability of self-consolidating concrete incorporating high-volume replacement composite cements, Cem. Concr. Res. 34 (11) (2004) 2103–2112, https://doi.org/10.1016/j.cemconres.2004.03.018.
[5] H. Okamura, K. Ozawa, M. Ouchi, Self-compacting concrete, Struct. Concr. 1 (1) (2000) 3–17. ⟨https://doi/abs/10.1680/stco.2000.1.1.3⟩.
[6] H. Okamura, K. Ozawa, Self-compactable high-performance concrete in Japan, Spec. Publ. 159 (1996) 31–44, https://doi.org/10.14359/10052.
[7] M. Elsayed, B.A. Tayeh, Y.I.A. Aisheh, et al., Shear strength of eco-friendly self-compacting concrete beams containing ground granulated blast furnace slag and fly ash as cement replacement, Case Stud. Constr. Mater. 17 (2022) e01354, https://doi.org/10.1016/j.cscm.2022.e01354.
[8] N. Bouzoubaå, M. Lachemi, Self-compacting concrete incorporating high volumes of class F fly ash: Preliminary results, Cem. Concr. Res. 31 (3) (2001) 413–420, https://doi.org/10.1016/S0008-8846(00)00504-4.
[9] G. Giakoumelis, D. Lam, Axial capacity of circular concrete-filled tube columns, J. Constr. Steel Res. 60 (7) (2004) 1049–1068, https://doi.org/10.1016/j.jcsr.2003.10.001.
[10] M.X. Xiong, J.Y.R. Liew, Fire resistance of high-strength steel tubes infilled with ultra-high-strength concrete under compression, J. Constr. Steel Res. 176 (2021) 106410, https://doi.org/10.1016/j.jcsr.2020.106410.
[11] X.H. Zhou, T.X. Xu, J.P. Liu, et al., Seismic performance of concrete-encased column connections for concrete filled thin-walled steel tube piers, Eng. Struct. 269 (2022) 114803, https://doi.org/10.1016/j.engstruct.2022.114803.
[12] W.Q. Hou, J.J. Yang, Z.X. Zhang, et al., Experimental study and application of manufactured sand self-compacting concrete in concrete-filled-steel-tube arch bridge: a case study, Case Stud. Constr. Mater. 15 (2021) e00718, https://doi.org/10.1016/j.cscm.2021.e00718.
[13] Y. Ouyang, J.J. Zeng, L.G. Li, et al., Influence of concrete mix proportions on axial performance of concrete-filled steel tubes made with self-compacting concrete, Adv. Struct. Eng. 23 (5) (2020) 835–846, https://doi.org/10.1177/1369433219884457.
[14] Y. Wang, L. Xiao, C. Jiang, et al., Axial loading behaviour of self-compacting concrete-filled thin-walled steel tubular stub columns, Adv. Civ. Eng. 2021 (2021) 1–7, https://doi.org/10.1155/2021/8861340.
[15] F. Yu, C. Qin, S. Wang, et al., Stress-strain relationship of recycled self-compacting concrete filled steel tubular column subjected to eccentric compression, Front. Struct. Civ. Eng. 14 (2020) 760–772, https://doi.org/10.1007/s11709-020-0618-3.
[16] M. Mahgub, A. Ashour, D. Lam, et al., Tests of self-compacting concrete filled elliptical steel tube columns, Thin-Walled Struct. 110 (2017) 27–34, https://doi.org/10.1016/j.tws.2016.10.015.
[17] L.H. Han, G.H. Yao, X.L. Zhao, Tests and calculations for hollow structural steel (HSS) stub columns filled with self-consolidating concrete (SCC), J. Constr. Steel Res. 61 (9) (2005) 1241–1269, https://doi.org/10.1016/j.jcsr.2005.01.004.
[18] J.J. Liao, Y.L. Li, Y. Ouyang, et al., Axial compression tests on elliptical high strength steel tubes filled with self-compacting concrete of different mix proportions, J. Build. Eng. 40 (2021) 102678, https://doi.org/10.1016/j.jobe.2021.102678.
[19] J.J. Liao, J.J. Zeng, Y.L. Long, et al., Behavior of square and rectangular concrete-filled steel tube (CFST) columns with horizontal reinforcing bars under eccentric compression, Eng. Struct. 271 (2022) 114899, https://doi.org/10.1016/j.engstruct.2022.114899.
[20] M. Ahmed, Q.Q. Liang, V.I. Patel, et al., Behavior of eccentrically loaded double circular steel tubular short columns filled with concrete, Eng. Struct. 201 (2019) 109790, https://doi.org/10.1016/j.engstruct.2019.109790.
[21] J. Ci, H. Jia, M. Ahmed, et al., Experimental and numerical analysis of circular concrete-filled double steel tubular stub columns with inner square hollow section, Eng. Struct. 227 (2021) 111400, https://doi.org/10.1016/j.engstruct.2020.111400.
[22] P. Ayough, N.H.R. Sulong, Z. Ibrahim, et al., Nonlinear analysis of square concrete-filled double-skin steel tubular columns under axial compression, Eng. Struct. 216 (2020) 110678, https://doi.org/10.1016/j.engstruct.2020.110678.
[23] P. Ayough, Y.H. Wang, W. Zeng, et al., Numerical investigation and design of concrete-filled double square steel tube columns under axial compression, J. Constr. Steel Res. 212 (2024) 108277, https://doi.org/10.1016/j.jcsr.2023.108277.
[24] W. Liang, J.F. Dong, S.C. Yuan, et al., Behavior of self-compacting concrete-filled steel tube columns with inclined stiffener ribs under axial compression, Strength Mater. 49 (2017) 125–132, https://doi.org/10.1007/s11223-017-9850-z.
[25] JGJ/T 283-2012. Technical Specification for Application of Self-compacting Concrete. Beijing: China State Engineering and Construction Press, 2012.

[26] Zhong S.T. Concrete-filled steel tube structure [M]. Beijing: Tsinghua University Press, 2003.
[27] Cai S.H. Modern concrete-filled steel tube structures [M]. Beijing: People's Communications Press, 2003.
[28] Han L.H. Concrete-filled steel tube structure-Theory and Practice (third edition). Beijing: Science Press, 2016.